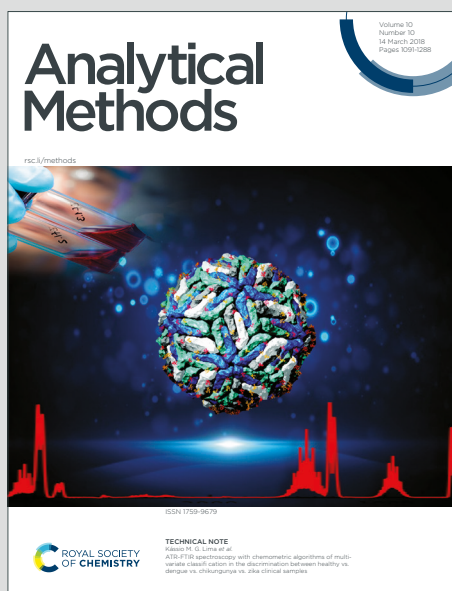


Analytical Methods

Accepted Manuscript

This article can be cited before page numbers have been issued, to do this please use: M. Shirani, Q. Salamat, M. jahanshahi, M. Soylak and S. Sepahi, *Anal. Methods*, 2026, DOI: 10.1039/D6AY00202A.



This is an Accepted Manuscript, which has been through the Royal Society of Chemistry peer review process and has been accepted for publication.

Accepted Manuscripts are published online shortly after acceptance, before technical editing, formatting and proof reading. Using this free service, authors can make their results available to the community, in citable form, before we publish the edited article. We will replace this Accepted Manuscript with the edited and formatted Advance Article as soon as it is available.

You can find more information about Accepted Manuscripts in the [Information for Authors](#).

Please note that technical editing may introduce minor changes to the text and/or graphics, which may alter content. The journal's standard [Terms & Conditions](#) and the [Ethical guidelines](#) still apply. In no event shall the Royal Society of Chemistry be held responsible for any errors or omissions in this Accepted Manuscript or any consequences arising from the use of any information it contains.

19 Abstract

20 In this study, a novel magnetic chitosan/zeolitic imidazolate frameworks-L /kiwi peel-derived
21 carbon dots (MCS/ZIF-L/KCDs) granular-leaf hybrid nanocomposite was synthesized and used
22 for magnetic dispersive μ solid-phase extraction (MD- μ SPE) of aflatoxins B1, B2, G1, and G2,
23 and the extracts were analyzed by high-performance liquid chromatography with fluorescence
24 detection (HPLC-FLD). The sorbent was characterized using Fourier-transform infrared
25 spectroscopy, X-ray diffraction, scanning electron microscopy, and energy-dispersive X-ray
26 spectroscopy. The influential parameters were optimized, and under optimum conditions, the
27 developed method showed excellent analytical performance with limits of detection (LOD) of
28 0.002–0.003 $\mu\text{g kg}^{-1}$, limits of quantification (LOQ) of 0.007–0.009 $\mu\text{g kg}^{-1}$, and linear dynamic
29 ranges (LDR) of 0.01–750 and 0.01–1000 $\mu\text{g kg}^{-1}$, depending on the analyte and matrix. The
30 relative recoveries (%) of 91.0–99.4, the intra-day (n=6) and inter-day (5 days, n=3) precisions at
31 $\leq 3.5\%$ and $\leq 3.0\%$, were acquired, respectively, which confirmed satisfactory capability,
32 reproducibility, and repeatability. The proposed method presented good compliance with green
33 analytical chemistry rules.

34
35 **Keywords:** ZIF-L; Carbon dots; Magnetic chitosan; Magnetic dispersive μ -Solid Phase
36 Extraction; Mycotoxins.

1. Introduction

Aflatoxins are a class of dangerous mycotoxins engendered by certain types of *Aspergillus* fungi, especially *Aspergillus flavus* and *Aspergillus parasiticus*¹. These toxins are primarily found in agricultural products such as cereals, seeds, and nuts, and they seriously affect human and animal health². Aflatoxin B and G are among the most important and common types of aflatoxins. Aflatoxin B1 is recognized as the most potent and carcinogenic kind, typically found in grains such as corn, wheat, and rice³. Similarly, Aflatoxin G1 is also hazardous and is produced under similar conditions. These toxins can be transmitted through the food chain to humans, posing significant risks to public health, including liver diseases, cancer, and immune disorders⁴. Controlling aflatoxin contamination in cereals is a major challenge for the agricultural and food industries⁵. Environmental conditions such as humidity and temperature can influence the production of these toxins; therefore, careful monitoring and appropriate management during the cultivation, harvesting, and storage of grains are essential⁶. Additionally, regulatory agencies have established maximum allowable limits for aflatoxins to protect consumer health⁷. The following decades saw the development of detection methods such as HPLC and GC, with organizations like the FDA and WHO establishing safety standards in the 1970s⁸. Today, monitoring of aflatoxins in food products has become a global focus due to increased trade, with ongoing research aimed at reducing health risks associated with these toxins⁹. Various analytical techniques have been applied. However, owing to the very low concentration of aflatoxins in food samples, application of a susceptible analytical method is essential, which requires the combination of an intense sample treatment method and a sensitive analytical technique¹⁰. Magnetic solid-phase extraction (MSPE) is an effective method for extracting aflatoxins B and G from various samples¹¹. This process involves preparing magnetic adsorbents, often iron oxide particles that are coated to enhance

1
2
3
4
5
6
7
8
9
10
11
12
13
14
15
16
17
18
19
20
21
22
23
24
25
26
27
28
29
30
31
32
33
34
35
36
37
38
39
40
41
42
43
44
45
46
47
48
49
50
51
52
53
54
55
56
57
58
59
60
This article is licensed under a Creative Commons Attribution-NonCommercial 3.0 Unported Licence.
Open Access Article. Published on 14 March 2016. Downloaded on 4/23/2016 10:14:02 PM.
This article is licensed under a Creative Commons Attribution-NonCommercial 3.0 Unported Licence.


1
2
3
4 63 selectivity ¹². Samples such as grains or dairy products are collected and processed to optimize
5
6 64 adsorption conditions. After mixing the sample with the adsorbent, a magnet is used to separate
7
8 65 the adsorbent containing aflatoxins ¹³. The adsorbent is then washed, and aflatoxins are eluted with
9
10 66 suitable solvents before being analyzed using atomic/emission spectrometry, high-performance
11
12 67 liquid chromatography (HPLC) ¹⁴, or gas chromatography (GC). MSPE offers advantages such as
13
14 68 high sensitivity, reduced extraction time, and lower contamination risk, but requires specialized
15
16 69 equipment and may incur higher initial costs. Overall, it is a valuable technique for assessing food
17
18 70 safety and quality. Quantum dots ¹⁵ and zeolitic imidazolate frameworks (ZIFs) ¹⁶ are effective
19
20 71 materials used for extraction and separation processes. Quantum dots are semiconductor
21
22 72 nanoparticles known for their high sensitivity, stability, and tunable properties, allowing them to
23
24 73 selectively identify target compounds such as toxins and drugs ¹⁷. ZIFs, which are constructed as
25
26 74 porous materials, provide large pores, selectivity, and thermal stability, making them suitable for
27
28 75 gas separation, water purification, and nutrient extraction ¹⁸. Combining quantum dots with ZIFs
29
30 76 enhances sensitivity and opens new applications in environmental sensing and drug detection. The
31
32 77 synthesis of these materials involves precise control over conditions and components, including
33
34 78 metal salts, ligands, and precursors of quantum dots ¹⁹. Overall, these materials promise
35
36 79 advancements in materials science and analytical chemistry. The synthesis of zeolitic imidazolate
37
38 80 frameworks (ZIFs) with quantum dots involves several precise steps. The main raw materials
39
40 81 include metal salts (e.g., $Zn(NO_3)_2$), ligands (e.g., 2-methylimidazole), quantum dot precursors
41
42 82 (such as CdSe), and solvents. This process includes the synthesis of quantum dots by dissolving
43
44 83 precursors, heating, cooling, and washing. Subsequently, ZIFs are formed by mixing metal and
45
46 84 ligand solutions with quantum dots, followed by incubation at controlled temperatures. The final
47
48 85 stages involve filtering, washing, and drying the product. Using zinc imidazolate frameworks (ZIF)

Open Access Article. Published on 14 May 2026. Downloaded on 6/20/26 10:14:02 PM.
This article is licensed under a Creative Commons Attribution-NonCommercial 3.0 Unported Licence.



1
2
3 86 as a quantum dot adsorbent for the adsorption of aflatoxins B and G presents a novel approach in
4
5 87 analytical chemistry, leveraging their porous structure and strong adsorption features. In recent
6
7 88 years, different MOF- and ZIF-based materials have been investigated for aflatoxin extraction,
8
9 89 removal, and detection. In addition, related chitosan/MOF composites and MOF/carbon-dot
10
11 90 systems have also been reported in the literature for aflatoxin-related applications^{20–23}. Therefore,
12
13 91 the novelty of the present study is not the general use of magnetic MOF/ZIF sorbents alone. Rather,
14
15 92 this work introduces a hierarchical MCS/ZIF-L/KCDs nanocomposite in which magnetic chitosan
16
17 93 provides magnetic separability and a biopolymeric support, ZIF-L supplies a leaf-like porous
18
19 94 framework with abundant accessible adsorption sites, and KCDs enrich the surface with additional
20
21 95 oxygen-containing functional groups and structural heterogeneity. To the best of our knowledge,
22
23 96 this specific MCS/ZIF-L/KCDs ternary sorbent has not been previously applied to the
24
25 97 simultaneous magnetic dispersive micro-solid phase extraction of aflatoxins B1, B2, G1, and G2
26
27 98 from ziziphus jujube, wheat, corn, white rice, pistachio, and walnut samples before HPLC-FLD
28
29 99 analysis.

100 2. Experimental

101 2.1. Chemicals

102 Aflatoxins B1, B2, G1, and G2 standards were purchased from Sigma Chemical Company (St.
103 Louis, MO, USA). A working standard solution (10 $\mu\text{g L}^{-1}$) was prepared by serial dilution in
104 deionized water. Phosphate Buffered Saline (PBS) tablets (pH 7.4) were obtained from Sigma-
105 Aldrich (USA). High-performance liquid chromatography (HPLC) grade solvents, including
106 methanol, acetonitrile, acetone, and ethyl acetate, were purchased from Merck (Germany). For the
107 synthesis of the nanocomposites, chitosan (low molecular weight), iron(III) chloride hexahydrate
108 ($\text{FeCl}_3 \cdot 6\text{H}_2\text{O}$), ammonium acetate (NH_4Ac), and sodium citrate tribasic dihydrate

1
2
3 109 (C₆H₅Na₃O₇·2H₂O) were used as precursors for the preparation of magnetic chitosan nanospheres
4
5 110 (MCS) and were purchased from Sigma-Aldrich (Germany). Ethylene glycol was used as the
6
7 111 reaction solvent for the MCS synthesis. Zinc nitrate hexahydrate (Zn(NO₃)₂·6H₂O) and 2-
8
9 112 methylimidazole (2-MIM), used for the growth of ZIF-L nanosheets, were also obtained from
10
11 113 Sigma-Aldrich. Methanol was used as the dispersion medium during the synthesis of MCS/ZIF-L.

12
13
14
15 114 To prepare kiwi peel-derived carbon dots (KCDs), fresh kiwi fruit was purchased from a local
16
17 115 market in Isfahan, Iran. Ethanol and deionized water (1:1, v/v) were used as the hydrothermal
18
19 116 solvent for KCDs synthesis. Syringe filters (0.2 μm pore size) used for the purification of the
20
21 117 KCDs solution were purchased from Sartorius (Germany).

2.2. Instrumentation

22
23
24
25
26
27
28
29
30
31
32
33
34
35
36
37
38
39
40
41
42
43
44
45
46
47
48
49
50
51
52
53
54
55
56
57
58
59
60

119 Analytical HPLC (Dinox, USA) with an autosampler (ASI-100 Dinox, USA), quaternary pump
120 (P680A, USA), fluorescence detector (model 170U, Dinox, USA), C18 column (10 cm length and
121 4.6 mm inner diameter ODS2 column), equipped with a Kobra cell, was used for chromatographic
122 analysis of aflatoxins B1, B2, G1, and G2. The mixture of MeOH: H₂O: ACN (400: 600: 60 v/v)
123 with potassium bromide (0.0131 g), and nitric acid (383 μL) was utilized as an isocratic mobile
124 phase. The column temperature and the mobile phase flow rate were set at 25 °C and 1.2 mL min⁻¹,
125 respectively. The detector was set at the emission wavelength of 440 nm and the excitation
126 wavelength of 360 nm. Fourier transform infrared (FT-IR) spectroscopy (Perkin-Elmer Range
127 400 spectrometer, Waltham, MA, USA) was used to identify the functional groups on the surface
128 of the sorbent. An instrument with a step size of 0.262606 from XRD-BRUKER AXS D8
129 ADVANCE, Türkiye, was used for X-ray diffraction (XRD). Surface morphology was examined
130 using a field-emission scanning electron microscope (FE-SEM, ZEISS Crossbeam 550, Germany).

131 2.3. Sample preparation

132 Ziziphus jujube, wheat, corn, white rice, pistachio, and walnut were bought from a local
133 grocery store in Isfahan, Isfahan Province, Iran. To prepare the real samples, the following
134 procedure was carried out:

135 5.0 g of each sample (ziziphus jujube powder, wheat, corn, and white rice) was weighed and
136 transferred to a 50 mL Falcon tube, then 0.5 g sodium chloride, 24 mL methanol, and 6 mL HPLC
137 water were added, and the mixture was vortexed in the dark for 10 min. Then, it was centrifuged
138 at 6500 rpm for 10 min. 3 mL of the upper phase was passed through a glass filter (0.1 micron).
139 The filtrate was diluted to 25 mL with PBS solution.

140 For the pistachio and walnut samples, the slurry should first be prepared. 5 g of each sample
141 was added to a 50 mL Erlenmeyer flask, and 0.25 g sodium chloride, 15 mL methanol, and 5 mL
142 n-hexane were added, and the mixture was vortexed in the dark for 5 min. The mixture was
143 centrifuged, and the 2.5 mL upper phase was filtered through a glass filter and then diluted to 25
144 mL with PBS solution. The prepared solution for all samples was used for the analytical process.


145 2.4. Synthesis Procedure of MCS/ZIF-L/KCDs Nanocomposites

146 2.4.1. KCDs Preparation

147 KCDs were synthesized through an environmentally friendly, single-step hydrothermal
148 approach utilizing desiccated kiwi peel²⁴. At the outset, fresh kiwi peels were thoroughly washed
149 with tap water to remove adhering pulp residues and surface impurities, and then rinsed several
150 times with deionized water to eliminate any remaining contaminants. The cleaned peels were
151 subsequently dried in an oven at 60 °C until a constant weight was achieved and then ground into
152 a fine powder. After that, 4 g of the dried biomass was dispersed in 60 mL of a water-ethanol
153 mixture (1:1, v/v). The resulting suspension was vigorously stirred and subjected to hydrothermal

1
2
3
4
5
6
7
8
9
10
11
12
13
14
15
16
17
18
19
20
21
22
23
24
25
26
27
28
29
30
31
32
33
34
35
36
37
38
39
40
41
42
43
44
45
46
47
48
49
50
51
52
53
54
55
56
57
58
59
60

Open Access Article. Published on 14 May 2026. Downloaded on 4/22/2026 10:14:02 PM.
This article is licensed under a Creative Commons Attribution-NonCommercial 3.0 Unported Licence.



1
2
3 154 treatment at 120 °C for 24 h. After cooling to room temperature, a yellow solution with a visible
4
5 155 precipitate was obtained. The suspension was carefully decanted to separate the dark yellow
6
7 156 insoluble precipitate, and the supernatant was filtered through a 0.2 µm syringe filter to obtain a
8
9 157 clear yellow carbon dot solution ²⁵.
10

158 2.4.2. Synthesis of MCS

159 Nanospheres of MCS were manufactured using a solvothermal method, incorporating changes
160 to previously documented procedures ²⁶. Initially, 100 mg of chitosan was dissolved in 100 mL of
161 ethylene glycol while being mechanically stirred to achieve a homogeneous solution. A mixture
162 of metal precursors comprising 2.4 g of FeCl₃·6H₂O (9.0 mmol), 1.39 g of NH₄Ac (18 mmol), and
163 0.85 g of C₆H₉Na₃O₉ (2.9 mmol) was gradually incorporated into the chitosan dispersion and
164 manually agitated for 15 min to attain a homogenous mixture. The ultimate solution was placed in
165 a Teflon-lined autoclave and underwent heat treatment at 190 °C for 16 hours. Upon natural
166 cooling to ambient temperature, a black precipitate was generated, which was subsequently
167 isolated and rinsed multiple times with ethanol and deionized water until the supernatant appeared
168 clear. The washed product (MCS) was subsequently dried in an oven at 60 °C overnight and kept
169 for future use.
39
40
41
42

170 2.4.3. Synthesis of MCS/ZIF-L/KCDs Granular-Leaf Hybrid Nanocomposites

171 To synthesize MCS/ZIF-L nanosheets, 0.5 g of the previously synthesized MCS was
172 suspended in 40 mL of methanol and stirred for 10 min. Following this, 2.2 g of 2-methylimidazole
173 (2-MIM, 26.8 mmol) and 3.0 g of Zn(NO₃)₂·6H₂O (3.35 mmol) were introduced to the suspension,
174 which was then stirred for 4.0 hours. To facilitate the creation of ZIF-L nanosheets on the MCS
175 surface, the reaction was placed under static conditions for 12 hours. The MCS/ZIF-L composite
56
57
58
59
60

1
2
3
4
5
6
7
8
9
10
11
12
13
14
15
16
17
18
19
20
21
22
23
24
25
26
27
28
29
30
31
32
33
34
35
36
37
38
39
40
41
42
43
44
45
46
47
48
49
50
51
52
53
54
55
56
57
58
59
60

Open Access Article. Published on 16 March 2026. Downloaded on 4/6/2026 10:14:02 PM.
This article is licensed under a Creative Commons Attribution-NonCommercial 3.0 Unported Licence.



1
2
3 176 (Product A) was obtained by magnetically isolating the product, washing it with methanol, and
4
5 177 then vacuum-drying it for 12 hours at 60°C²⁷.

6
7
8 178 To synthesize the ternary nanocomposite of MCS/ZIF-L/KCDs, 0.5 g of the MCS/ZIF-L
9
10 179 composite (Product A) was dispersed in 50 mL of a previously produced KCDs solution. The
11
12 180 mixture was mechanically stirred at room temperature for 24 hours to ensure uniform loading of
13
14 181 KCDs onto the ZIF-L-modified MCS. The final product was extracted using a magnet, thoroughly
15
16 182 purified with ethanol, and subjected to vacuum drying at 60 °C for 12 hours to produce the
17
18 183 MCS/ZIF-L/KCDs nanocomposite.

184 2.5. pH of the Isoelectric Point

185 The pH of the point of zero charge (pH_{PZC}) represents the pH at which the net surface charge
186 of a material is zero, meaning that the positive and negative charges on the sorbent surface are
187 balanced. At this pH, the material exhibits minimal electrostatic interaction with surrounding
188 species due to the absence of an overall surface charge. To determine the pH_{PZC} of the MCS/ZIF-
189 L/KCDs nanocomposite, 10 mL of 0.1 mol L⁻¹ sodium nitrate (NaNO₃) solution was transferred
190 into twelve Falcon tubes. The initial pH values were adjusted in the range of 1–12 using dilute HCl
191 or NaOH solutions. Subsequently, 10 mg of the nanocomposite was added to each tube. The
192 suspensions were shaken for 24 h to reach equilibrium. After equilibration, the final pH values
193 were measured, and the difference between the initial and final pH values (ΔpH) was calculated.
194 The ΔpH values were plotted against the initial pH, and the point where the curve crossed ΔpH =
195 0 was taken as the pH_{PZC}. As shown in Fig. S1, the pH_{PZC} of the MCS/ZIF-L/KCDs sorbent was
196 found to be 7.3, indicating that the sorbent surface is nearly electrically neutral around
197 physiological pH.

198 2.6. Analytical Procedure

199 The volume of 25 mL sample solution was transferred to a Falcon tube, and the amount 30 mg
200 of MCS/ZIF-L/KCDs was added to it and vortexed for 2 min to ensure efficient and rapid
201 interaction between sorbent and analytes for preconcentration. Owing to the magnetic property of
202 the nanostructure sorbent, MCS/ZIF-L/KCD were separated from the solution using an external
203 magnet, and the upper phase was removed completely. 100 μ L methanol was used to elute analytes
204 from the sorbent after 90 s sonication. Then, an external magnet was utilized to separate the
205 magnetic nanocomposite. The methanol containing aflatoxins B1, B2, G1, and G2 was analyzed
206 with HPLC-FLD. The calibration curves were acquired via the matrixed match method.

207 3. Results and Discussion

208 3.1. Characterization

209 The synthesis and structural evolution of the MCS, MCS/ZIF-L, and MCS/ZIF-L/KCDs
210 composites were validated using various complementary characterization techniques. The analyses
211 conducted using FTIR and XRD validated the chemical functionalities and crystalline changes at
212 each stage of production. To investigate morphological evolution, SEM was utilized, uncovering
213 unique surface topologies for each material. Furthermore, EDX was conducted to ascertain the
214 elemental content and distribution within the composites, offering additional confirmation of the
215 successful integration of each component (Fig. 1).

216 The FTIR spectra of MCS (Fig. 1 (a)) exhibit a large band about $\sim 3400\text{ cm}^{-1}$, indicative of the
217 O–H and N–H stretching vibrations from chitosan and adsorbed water. Peaks detected at around
218 2920 and 2850 cm^{-1} are ascribed to C–H stretching vibrations of aliphatic $-\text{CH}_2$ groups. The peak
219 at around 1640 cm^{-1} is attributed to N–H bending or amide I, whereas the range of $1100\text{--}1030\text{ cm}^{-1}$



1
2
3 220 ¹ is associated with C–O–C stretching of glycosidic bonds. A prominent band at approximately
4
5 221 570 cm⁻¹ signifies Fe–O stretching, hence validating the integration of Fe₃O₄ nanoparticles into
6
7 222 the magnetic chitosan matrix. In the MCS/ZIF-L composite, distinct peaks at approximately 1570–
8
9 223 1470 cm⁻¹ belong to C=N and C=C stretching vibrations, whilst peaks at around 1350–900 cm⁻¹
10
11 224 are ascribed to C–N stretching and aromatic C–H bending within the imidazole rings of ZIF-L.
12
13 225 The Zn–N stretching vibration at around 430–450 cm⁻¹ further corroborates the effective synthesis
14
15 226 of the ZIF-L framework. The –OH/NH band exhibits a modest decrease in intensity and a shift,
16
17 227 signifying coordination interactions between the functional groups of chitosan and the ZIF-L
18
19 228 network²⁸. The final MCS/ZIF-L/KCDs composite exhibits additional alterations. The substantial
20
21 229 hydrogen bonding is indicated by the increased intensity of the broad –OH/NH band about ~3400
22
23 230 cm⁻¹, attributed to the surface –OH and –COOH groups of the KCDs. A novel peak at
24
25 231 approximately 1720 cm⁻¹ is attributed to the C=O stretching vibration of carboxylic groups on
26
27 232 KCDs, whereas bands at around 1620 and 1400 cm⁻¹ correspond to C=C and C–H bending,
28
29 233 respectively. The C–O–C stretching reemerges at approximately 1100 cm⁻¹, corroborating the
30
31 234 existence of oxygenated groups from KCDs. The continued presence of Fe–O and Zn–N bands in
32
33 235 the composite spectra confirms the structural integrity of the magnetic and ZIF-L components²⁹.

34
35
36 236 Additional insights from XRD analysis (Fig. 1 (b)) further support the sequential construction
37
38 237 of the composite. The MCS pattern demonstrates broad diffraction at approximately 20–25° (2θ),
39
40 238 indicating the amorphous nature of chitosan. In contrast, distinct peaks at approximately 30.1°,
41
42 239 35.4°, 43.3°, 53.7°, 57.0°, and 62.6° are associated with the (220), (311), (400), (422), (511), and
43
44 240 (440) planes of crystalline Fe₃O₄, following JCPDS card no. 19-0629³⁰. The inclusion of ZIF-L
45
46 241 results in the emergence of distinct peaks at approximately 11.7°, 13.1°, 17.0°, 22.2°, 24.6°, 26.7°,
47
48 242 and 29.9°, which correspond to the unique diffraction pattern of ZIF-L. This confirms the effective
49
50
51
52
53
54
55
56
57
58
59
60

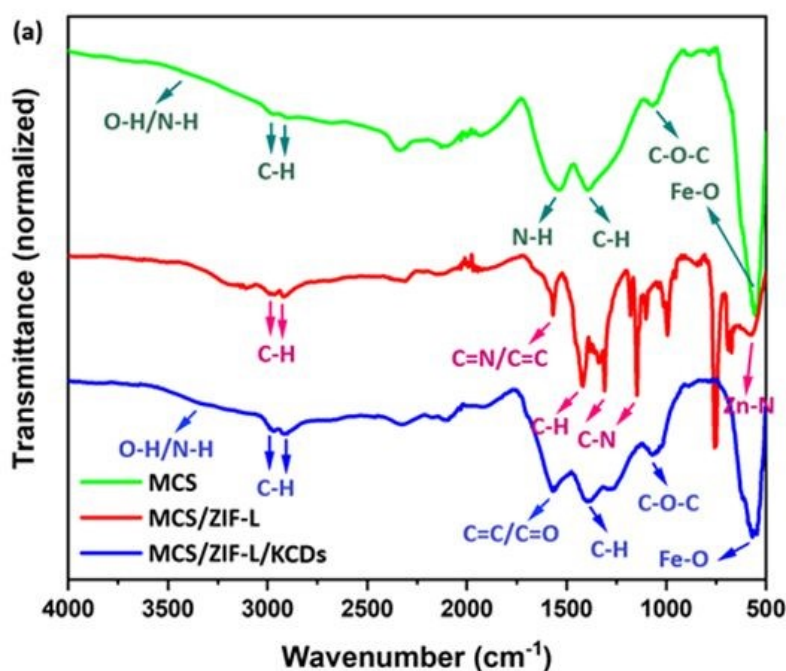
1
2
3 243 crystallization of the ZIF-L structure on the MCS surface ²⁸. The resulting MCS/ZIF-L/KCDs
4
5 244 composite exhibits a significant broadening of peaks and an overall reduction in intensity. The
6
7 245 prominence of the hump in the $\sim 20\text{--}30^\circ$ range is enhanced by the semi-crystalline or amorphous
8
9 246 characteristics of KCDs. Although certain reflections from ZIF-L persist, their diminished
10
11 247 intensity and minor displacements suggest structural distortion and obscuration by CDs ³¹.

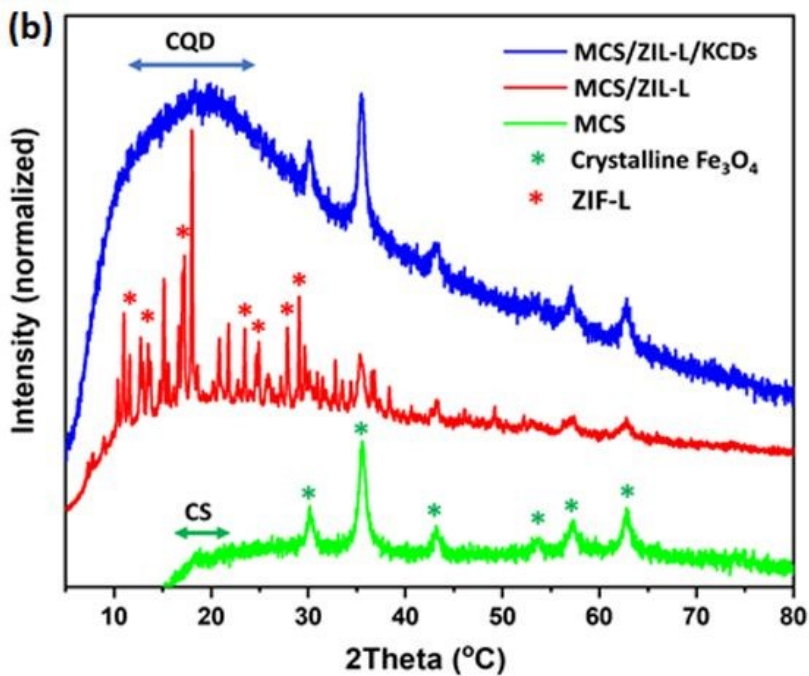
12
13
14 248 The SEM images (Fig. 1 (c)) show that the pristine MCS (Images i–iii) displays a consistent,
15
16 249 spherical morphology, with particle sizes ranging from sub-micron to several microns in diameter.
17
18 250 Images (i) and (ii) show spherical particles that are smooth and densely packed, suggesting
19
20 251 effective dispersion of Fe₃O₄ nanoparticles within the chitosan matrix. Higher magnification
21
22 252 (image iii) reveals the fine, textured surfaces of individual microspheres, which could provide
23
24 253 active sites for surface interactions. The spherical shape is consistent with literature reports of
25
26 254 magnetically induced self-assembly of chitosan-based composites ³². Upon the growth of the ZIF-
27
28 255 L framework on the MCS surface (MCS/ZIF-L), significant morphological changes are observed.
29
30 256 Images (iv) and (v) display the formation of leaf-like crystalline platelets, which are typical of ZIF-
31
32 257 L's two-dimensional structure. These platelets are radially grown and appear densely anchored on
33
34 258 the surface of the MCS spheres, creating a rough, flower-like composite architecture. The graph
35
36 259 in (vi) demonstrates that the spherical MCS particles are visible beneath the ZIF-L layer, hence
37
38 260 proving the successful occurrence of heterogeneous nucleation. This hierarchical structure is
39
40 261 expected to enhance the surface area and active sites, hence improving adsorption or catalytic
41
42 262 applications ³³. The addition of KCDs further alters the surface properties, as illustrated in images
43
44 263 (vii) to (ix) (MCS/ZIF-L/KCDs). The overall structure exhibits a rougher and more granular
45
46 264 quality, with the leaf-like characteristics largely hidden beneath a chaotic, delicate layer. This
47
48 265 coating is associated with KCDs aggregates that enhance and potentially connect the ZIF-L
49
50
51
52
53
54
55
56
57
58
59
60

1
2
3 266 platelets. The nanoscale granular features displayed by KCDs are visible in the high-magnification
4
5 267 images (viii and ix), indicating successful deposition and surface functionalization. The KCDs
6
7 268 demonstrate the ability to enhance conductivity, dispersibility, and the availability of functional
8
9 269 groups on the composite surface ²⁹.

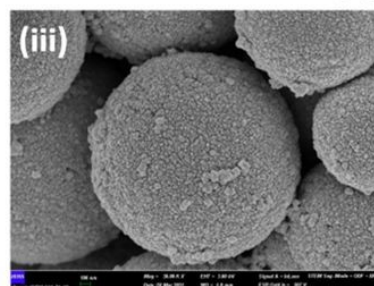
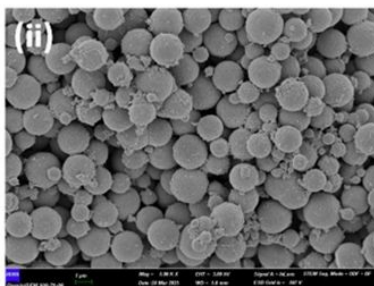
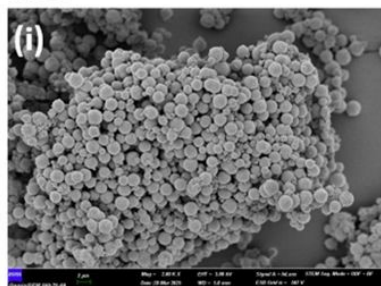
10
11 270 Regarding the SEM-EDX images (Fig. 1 (d)), the spectrum of the MCS composite (image i)
12
13 271 shows the presence of carbon (C), nitrogen (N), oxygen (O), and a prominent signal from iron
14
15 272 (Fe). The increased Fe content (62.62 wt%) confirms the successful incorporation of Fe₃O₄
16
17 273 nanoparticles into the chitosan matrix. The significant peaks of C (17.96 wt%) and O (16.24 wt%)
18
19 274 arise from the chitosan backbone and the adsorbed functional groups, whereas N (3.18 wt%)
20
21 275 signifies the presence of amine groups derived from deacetylated chitosan. The findings
22
23 276 correspond with established literature and confirm the effective synthesis of the MCS support,
24
25 277 demonstrating magnetic characteristics. The elemental profile in the MCS/ZIF-L composite, as
26
27 278 illustrated in image ii, undergoes significant alteration with the addition of ZIF-L to the MCS
28
29 279 support. A significant increase in C (28.64 wt%) and N (15.48 wt%) is observed, both indicating
30
31 280 the incorporation of the 2-MIM linker in the synthesis of ZIF. The appearance of Zn peaks (13.84
32
33 281 wt%) along with a reduction in Fe (30.14 wt%) indicates partial surface coverage of the MCS
34
35 282 spheres by ZIF-L crystals. The Zn: Fe ratio supports the effective growth of ZIF-L onto the
36
37 283 magnetic chitosan surface. The enhanced nitrogen content also confirms the introduction of
38
39 284 nitrogen-rich imidazole groups, validating the formation of the ZIF framework. After the
40
41 285 integration of KCDs, the EDX profile of the MCS/ZIF-L/KCDs composite (picture iii) indicates a
42
43 286 notable increase in carbon content (29.84 wt%), aligning with the carbonaceous characteristics of
44
45 287 KCDs. The Fe signal (44.25 wt%) persists, suggesting the preservation of the core magnetic
46
47 288 structure. The Zn concentration (4.86 wt%) is significantly lower than that observed in the
48
49
50
51
52
53
54
55
56
57
58
59
60

289 MCS/ZIF-L stage, likely due to inadequate coverage of the ZIF-L surface by KCDs. The identified
290 contributions of O (16.73 wt%) and N (4.32 wt%) are attributed to oxygenated functional groups
291 and nitrogen doping commonly observed in KCDs, along with residual contributions from chitosan
292 and ZIF-L. The findings provide strong evidence for effective surface functionalization and
293 composite synthesis.



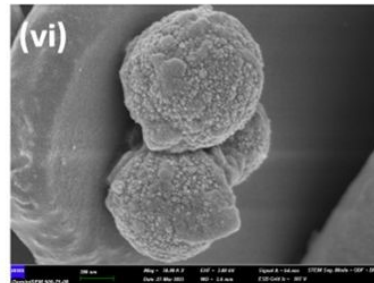
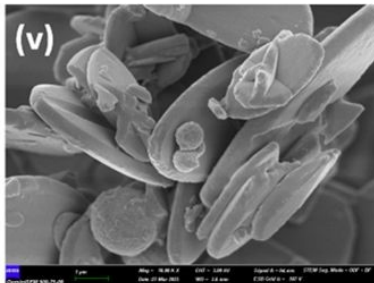
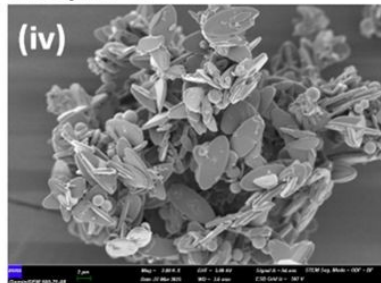


MCS

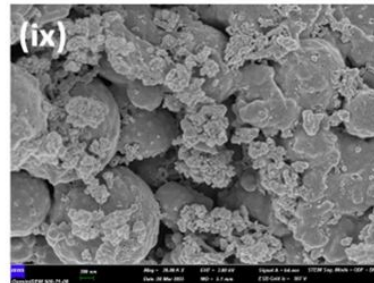
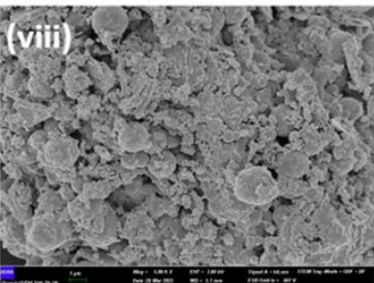
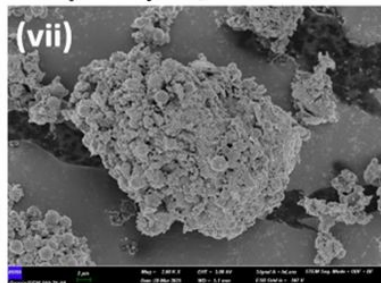


(c)

MCS/ZIF-L



MCS/ZIF-L/ KCDs



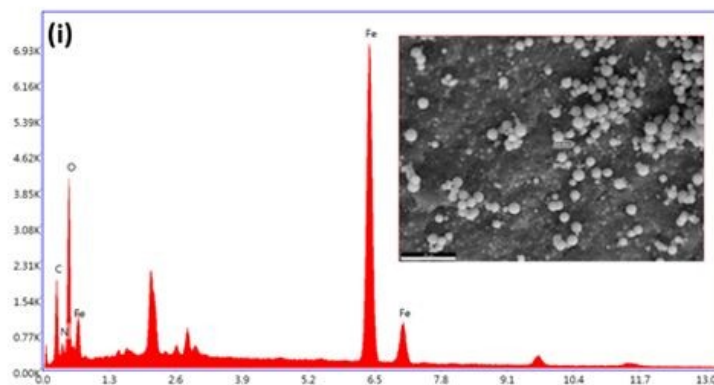
Analytical Methods Accepted Manuscript

1
2
3
4
5
6
7
8
9
10
11
12
13
14
15
16
17
18
19
20
21
22
23
24
25
26
27
28
29
30
31
32
33
34
35
36
37
38
39
40
41
42
43
44
45
46
47
48
49
50
51
52
53
54
55
56
57
58
59
60

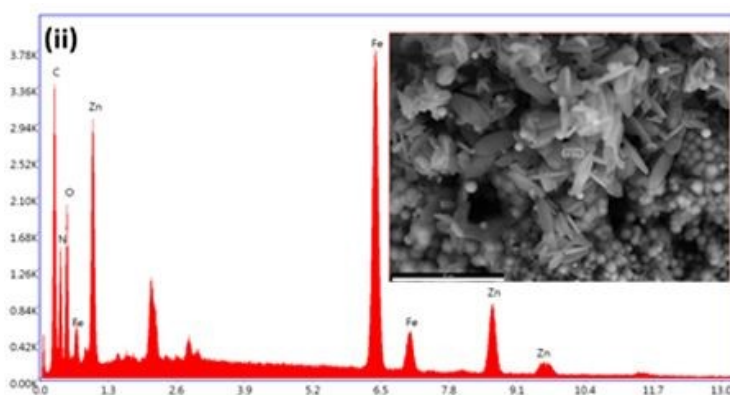
Open Access Article. Published on 16 March 2016. Downloaded on 16/03/2016 14:14:02. This article is licensed under a Creative Commons Attribution-NonCommercial 3.0 Unported Licence.



(d)



Element	Weight %	Atomic %	Net Int.
C K	17.96	38.75	337.05
N K	3.18	5.88	63.29
O K	16.24	26.3	800.65
FeK	62.62	29.06	3261.13



Element	Weight %	Atomic %	Net Int.
C K	28.64	47.84	641.76
N K	15.48	22.16	263.19
O K	11.9	14.92	382.37
FeK	30.14	10.83	1824.18
ZnK	13.84	4.25	429.8

1
2
3
4
5
6
7
8
9
10
11
12
13
14
15
16
17
18
19
20
21
22
23
24
25
26
27
28
29
30
31
32
33
34
35
36
37
38
39
40
41
42
43
44
45
46
47
48
49
50
51
52
53
54
55
56
57
58
59
60

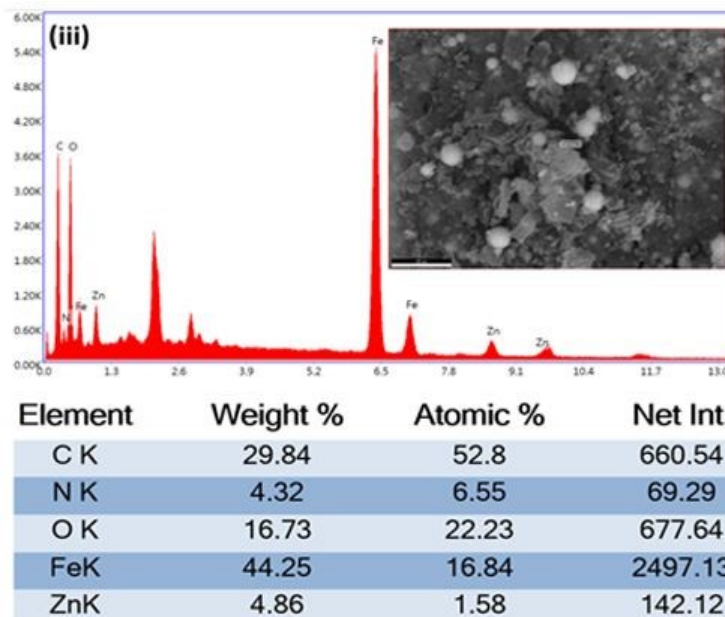


Fig. 1 (a) FTIR spectra of MCS, MCS/ZIF-L, and MCS/ZIF-L/KCDs nanocomposite, (b) XRD spectra of MCS, MCS/ZIF-L, and MCS/ZIF-L/KCDs nanocomposite, (c) SEM images of MCS (i-iii), MCS/ZIF-L (iv-vi), and MCS/ZIF-L/KCDs nanocomposite (vii-ix), (d) EDX spectra and the elemental composition of MCS (i), MCS/ZIF-L (ii), and MCS/ZIF-L/KCDs nanocomposite (iii).

294

295 3.2. Optimization of the MCS/ZIF-L/KCDs-MD- μ SPE Process

296 The acidity and basicity of the analyte solution affect both the analyte's functional groups and
 297 the sorbent's functional groups. To this goal, the pH of the solution was explored in the range of
 298 3-10, and as shown in Fig. 2 (a), the extraction recoveries enhanced from 3-7 and became constant
 299 from 7-8, and then decreased. Generally, aflatoxin structures can be hydrolyzed, and the lactonic
 300 ring may also be decomposed in strong basic or acidic media. Therefore, the interest in aflatoxins
 301 can be adsorbed on the surface of the MCS/ZIF-L/KCDs at neutral conditions via hydrogen
 302 bonding, π - π , and van der Waals interactions³⁴. To set the pH of the solution, PBS buffer solution
 303 (pH = 7.4) was used. This optimum pH is also consistent with the experimentally determined pH_{PZC}

304 value of 7.3 for the MCS/ZIF-L/KCDs sorbent (Fig. S1), suggesting favorable surface conditions
305 for the extraction of aflatoxins under near-neutral conditions.

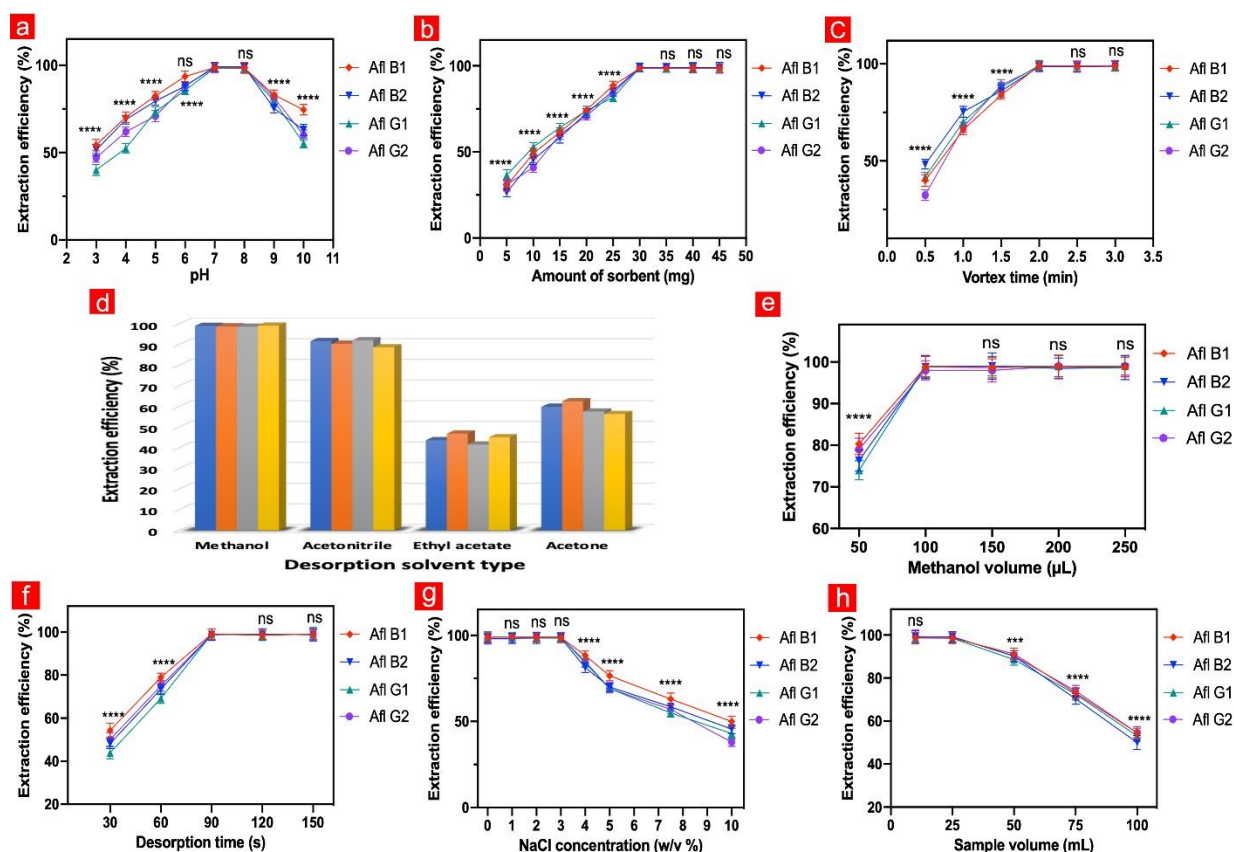


Fig. 2 The effect of influential parameters on the extraction efficiencies of aflatoxins: (a) pH, (b) amount of sorbent, (c) vortex time, (d) desorption solvent type, and (e) desorption solvent volume, (f) desorption time, (g) ionic strength, (h) sample volume; Data are represented as mean \pm SD based on three independent experiments and significant differences between groups appeared with (ns= not significant), *($P < 0.05$), **($P < 0.01$), ***($P < 0.001$), and ****($P < 0.0001$) using two-way ANOVA with Dunnett's multiple comparisons test, with individual variances computed for each comparison

306

307 The amount of adsorbent determines the number of available active sites for analyte
308 adsorption; therefore, increasing the sorbent dosage generally increases the number of accessible
309 adsorption sites. The adsorbent dosage was studied in the range of 5-40 mg, and the optimum
310 amount of 25 mg was attained Fig. 2 (b).

1
2
3
4
5
6
7
8
9
10
11
12
13
14
15
16
17
18
19
20
21
22
23
24
25
26
27
28
29
30
31
32
33
34
35
36
37
38
39
40
41
42
43
44
45
46
47
48
49
50
51
52
53
54
55
56
57
58
59
60

1
2
3 311 Vortex time supplies a qualified period of time for the analytes to be adsorbed on the surface of
4
5 312 the adsorbent. Therefore, vortex time was studied from 0.5 to 2.5 min, and as seen in Fig. 2 (c),
6
7 313 the time of 1.0 min was optimum and sufficient to allow the analyte adsorption and separation.
8
9 314 The desorption solvent type has an important role in the extraction efficiency. The desorption
10
11 315 solvent should establish a strong interaction with the analyte to elute and desorb it from the sorbent.
12
13 316 The effect of some desorption solvents, including methanol, acetone, acetonitrile, and ethyl
14
15 317 acetate, was investigated. As the results shown in Fig. 2 (d), methanol could desorb aflatoxins
16
17 318 more efficiently, which may be due to the higher polarity of methanol (via hydrogen bonding
18
19 319 interactions) and can interact with aflatoxin B1, B2, G1, and G2 as polar compounds. The order
20
21 320 of polarity indexes of the interest desorption solvents is methanol (6.6) > acetonitrile (6.2) >
22
23 321 acetone (5.4), respectively, which confirms the obtained results.

24
25 322 Preconcentration factor (PF) is assessed as the ratio of sample solution volume to desorption
26
27 323 solvent volume, and PF indicates the potency of the method to analyze trace/ultra-trace
28
29 324 concentrations with higher sensitivity. The methanol volume was observed for the volumes of 50
30
31 325 μL to 250 μL , and as shown in Fig. 2 (e), the extraction efficiencies for four analytes increased
32
33 326 from 50-100 μL and then became constant. Hence, the volume of 100 μL was selected as optimum
34
35 327 for the rest of the studies, and the PF of 250 was achieved.

36
37 328 The desorption time is influential in providing an appropriate time for the desorption solvent
38
39 329 to interact with the analyte and desorb it from the sorbent. The desorption time was explored from
40
41 330 30 s to 150 s, and as revealed in Fig. 2 (f), the desorption time of 90 s was chosen for the rest of
42
43 331 the studies.

44
45 332 The ionic strength of the solution is defined by adding a salt such as NaCl and is called the
46
47 333 salting-in effect or salting-out. The concentration of NaCl was studied from 0 to 10 % (w/v), and

Open Access Article. Published on 14 March 2016. Downloaded on 6/20/26 10:14:02 PM.
This article is licensed under a Creative Commons Attribution-NonCommercial 3.0 Unported Licence.
CC BY-NC

1
2
3 334 as indicated in Fig. 2 (g), the extraction efficiencies were constant and maximum from 0 - 3 % and
4
5 335 then decreased. It can be concluded that by the augmentation of the concentration of salt, the
6
7 336 viscosity of the solution increases, and the mass transfer of analytes from the solution to the surface
8
9 337 of the sorbent decreases. Moreover, the salt molecules can occupy the active sites of the sorbent
10
11 338 and lead to a decrease in extraction efficiencies.

12
13 339 Besides the desorption solvent volume, the volume of the sample solution also impacts the PF
14
15 340 and should be precisely determined. Therefore, the sample volume in the range 10-100 mL was
16
17 341 considered, and as indicated in Fig. 2 (h), the extraction efficiencies were maximum and
18
19 342 quantitative from 25 mL and then reduced. Hence, the sample volume of 25 mL was opted as
20
21 343 optimum.

22 344 **3.3. Adsorbent Reusability**

23
24 345 The regenerability of MCS/ZIF-L/KCDs clarifies the potential and the efficiency of the
25
26 346 sorbent. To this aim, the polluted adsorbent was mixed with 0.5 mL solution of methanol:
27
28 347 acetonitrile (50:50 (v/v %)). The clean sorbent could be reused with extraction efficiencies over
29
30 348 98 % and over 90 % after four and six washings, respectively, which shows the high capability of
31
32 349 MCS/ZIF-L/KCDs.

33 350 **3.4. Statistical Analysis**

34
35 351 Statistical analysis was performed using GraphPad Prism 6 software (USA). Data were
36
37 352 expressed as mean \pm standard deviation (SD). Two-way analysis of variance (ANOVA) followed
38
39 353 by Dunnett's multiple comparison test was applied as a supportive statistical tool to compare the
40
41 354 experimental conditions investigated during the optimization of the extraction procedure,
42
43 355 including solution pH, sorbent amount (mg), NaCl concentration (w/v %), methanol volume (μ L),
44
45
46
47
48
49
50
51
52
53
54
55
56
57
58
59
60

1
2
3 356 vortex time (min), desorption time (s), and sample volume (mL). The statistical analysis was used
4
5 357 only to confirm the observed trends in extraction efficiency, while the selection of the optimal
6
7 358 conditions was primarily based on the highest extraction recovery and practical considerations.
8
9
10

11 359 3.5. Green Evaluation Metrics of the Method

12 360 In recent years, several green metric tools have been developed to evaluate the environmental
13
14 361 impact of analytical procedures³⁵. The AGREE metric provides a visual and numerical assessment
15
16 362 of analytical greenness based on the principles of green analytical chemistry, using a color scale
17
18 363 from red to green with scores ranging from 0 to 1. The AGREE score obtained for the proposed
19
20 364 MCS/ZIF-L/KCDs-MD- μ SPE method was 0.66, indicating a moderate to good level of analytical
21
22 365 sustainability. As illustrated in Fig. 3(a), the results suggest that the developed method offers
23
24 366 environmental advantages mainly due to the low consumption of sorbent, reduced solvent
25
26 367 volumes, and rapid extraction procedure.

27 368 The AGREEprep tool was also applied to evaluate the greenness of the sample preparation
28
29 369 step. This metric considers ten evaluation criteria related to sample preparation, each expressed as
30
31 370 a sub-score between 0 and 1 and represented by color-coded segments. The AGREEprep score for
32
33 371 the proposed method was 0.59, reflecting an improved environmental profile compared with many
34
35 372 conventional extraction approaches (Fig. 3(b)).

36 373 In addition, the BAGI (Blue Analytical Greenness Index) was used as another complementary
37
38 374 green metric to assess the sustainability of the analytical procedure. The BAGI index evaluates
39
40 375 several parameters associated with analytical methods, including reagent toxicity, solvent
41
42 376 consumption, energy requirements, and waste generation, and represents the results through a blue-
43
44 377 scale pictogram. The BAGI score obtained for the proposed method was 62.5, as shown in Fig.
45
46 378 3(c), indicating an acceptable level of environmental performance according to this evaluation
47
48
49
50
51
52
53
54
55
56
57
58
59
60

Open Access Article. Published on 14 March 2026. Downloaded on 4/6/2026 10:14:02 PM.
This article is licensed under a Creative Commons Attribution-NonCommercial 3.0 Unported Licence.



379 approach. It should be noted that the use of organic solvents such as methanol and acetonitrile, as
 380 well as the solvothermal synthesis of the sorbent, still contribute to the environmental footprint of
 381 the method. Therefore, the obtained AGREE, AGREEprep, and BAGI scores should be interpreted
 382 as indicators of improved analytical sustainability rather than absolute greenness. Nevertheless,
 383 the reduced solvent consumption, short extraction time, and small sorbent requirement of the MD-
 384 μ SPE procedure contribute to minimizing the overall environmental impact of the analytical
 385 workflow.

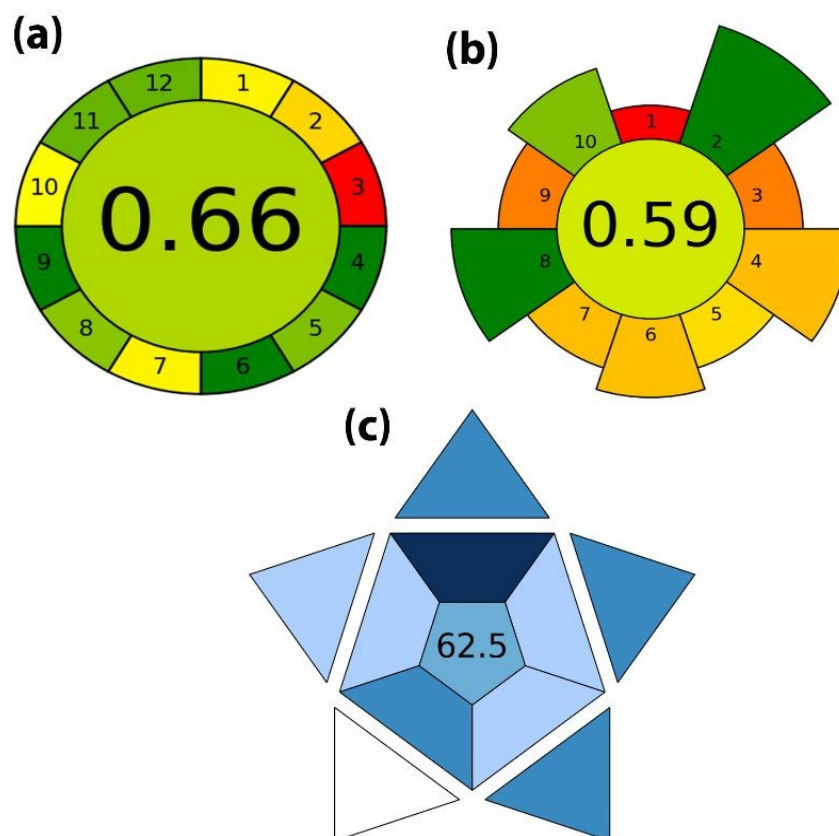


Fig. 3 The greenness evaluations of MCS/ZIF-L/KCDs -D μ SPE : (a) AGREE, (b) AGREEprep, (c) BAGI Index pictogram of the process

386

 1
2
3
4
5
6
7
8
9
10
11
12
13
14
15
16
17
18
19
20
21
22
23
24
25
26
27
28
29
30
31
32
33
34
35
36
37
38
39
40
41
42
43
44
45
46
47
48
49
50
51
52
53
54
55
56
57
58
59
60

388 3.6. Method validation

389 The analytical performance of the developed MCS/ZIF-L/KCDs-MD- μ SPE method was
390 evaluated under the optimized experimental conditions. The validation parameters included linear
391 dynamic range (LDR), limit of detection (LOD), limit of quantification (LOQ), relative standard
392 deviation (RSD), enrichment factor (EF), and coefficient of determination (R^2). As summarized in
393 Table 1, the proposed method demonstrated good linearity over concentration ranges of 0.01–750
394 $\mu\text{g kg}^{-1}$ and 0.01–1000 $\mu\text{g kg}^{-1}$, depending on the analyte and sample matrix. The limits of detection
395 (LOD) were calculated based on the $3S_b/m$ criterion, where S_b represents the standard deviation
396 of the blank signal and m denotes the slope of the calibration curve. The limits of quantification
397 (LOQ) were defined as the lowest concentration level that could be quantitatively determined with
398 acceptable accuracy and precision using the proposed method. The obtained LOD values ranged
399 from 0.002 to 0.003 $\mu\text{g kg}^{-1}$, while the LOQ values ranged from 0.007 to 0.009 $\mu\text{g kg}^{-1}$ for the
400 studied analytes in different food matrices. The precision of the method was evaluated in terms of
401 intra-day and inter-day repeatability by analyzing samples spiked at three concentration levels.
402 The obtained relative standard deviation (RSD) values were $\leq 3.0\%$ for intra-day precision and \leq
403 3.5% for inter-day precision, indicating satisfactory repeatability of the developed method. The
404 detailed analytical performance results are presented in Table 1.

1
2
3
4
5
6
7
8
9
10
11
12
13
14
15
16
17
18
19
20
21
22
23
24
25
26
27
28
29
30
31
32
33
34
35
36
37
38
39
40
41
42
43
44
45
46
47
48
49
50
51
52
53
54
55
56
57
58
59
60

Open Access Article. Published on 14 May 2026. Downloaded on 4/6/2026 10:14:02 PM.
This article is licensed under a Creative Commons Attribution-NonCommercial 3.0 Unported Licence.



Table 1 The analytical performance of MCS/ZIF-L/KCDs - MD- μ SPE process for simultaneous separation and preconcentration of aflatoxins B1, B2, G1, G2

LOD ($\mu\text{g kg}^{-1}$)				LOQ ($\mu\text{g kg}^{-1}$)				LDR ($\mu\text{g kg}^{-1}$)				Equation				R ²				EF			
B1	B2	G1	G2	B1	B2	G1	G2	B1	B2	G1	G2	B1	B2	G1	G2	B1	B2	G1	G2	B1	B2	G1	G2
0.003	0.003	0.002	0.003	0.009	0.007	0.008	0.009	0.01-750	0.01-1000	0.01-1000	0.01-750	Y=6.7333 X+0.8392	Y=12.353 X+0.8026	Y=7.7152 X+0.2041	Y=6.6156 X+0.5208	0.9990	0.9996	0.9993	0.9993	243.6	247.1	243.5	248.1
0.003	0.002	0.002	0.002	0.009	0.007	0.008	0.009	0.01-750	0.01-750	0.01-1000	0.01-500	Y=12.077 X+0.0821	Y=9.7287 X+0.2109	Y=7.9819 X+0.1016	Y=7.4337 X+0.1469	0.9992	0.9991	0.9996	0.9995	248.5	245.5	246.5	247.5
0.003	0.002	0.002	0.003	0.008	0.008	0.008	0.008	0.01-750	0.01-750	0.01-1000	0.01-750	Y=12.588 X+0.4711	Y=10.671 X-0.0874	Y=7.7101 X+0.851	Y=5.6313 X+0.1194	0.9964	0.9978	0.9992	0.9993	245.9	245.9	246.8	247.5
0.003	0.003	0.002	0.002	0.007	0.008	0.008	0.008	0.01-750	0.01-750	0.01-1000	0.01-500	Y=10.782 X+0.4904	Y=11.476 X+0.8116	Y=8.7333 X+0.9967	Y=7.9624 X+0.5598	0.9996	0.9988	0.9993	0.9998	246.5	248.1	244.2	246.3
0.003	0.003	0.003	0.002	0.008	0.008	0.008	0.008	0.01-750	0.01-750	0.01-750	0.01-500	Y=17.632 X+0.7932	Y=14.505 X+0.3775	Y=6.7923 X+0.3517	Y=6.2332 X+0.5613	0.9996	0.9981	0.9993	0.9973	246.3	241.6	244.5	243.0
0.003	0.002	0.003	0.002	0.009	0.008	0.008	0.009	0.01-750	0.01-500	0.01-750	0.01-500	Y=12.87 X+2.5296	Y=17.368 X+0.2024	Y=5.9607 X+0.1588	Y=7.9594 X+0.3235	0.9999	0.9990	0.9988	0.9982	242.7	243.8	247.1	244.8



Analytical Methods Accepted Manuscript

407

408 3.7. Extraction Mechanism

409 The efficient extraction of aflatoxins B1, B2, G1, and G2 by the MCS/ZIF-L/KCDs
410 nanocomposite can be attributed to the synergistic contributions of the physical, chemical, and
411 structural properties of the composite sorbent ³⁶. The hierarchical composite structure is designed
412 to integrate the advantages of its individual components, namely MCS, ZIF-L nanosheets, and
413 KCDs. The magnetic chitosan core provides a biocompatible and magnetically retrievable
414 substrate containing abundant hydroxyl and amine functional groups, which can participate in
415 hydrogen bonding and polar interactions with aflatoxin molecules. These functional groups
416 contribute to the affinity of the sorbent toward polar analytes while enabling convenient magnetic
417 separation of the sorbent from the sample solution.

418 The ZIF-L nanosheets grown on the MCS surface introduce a porous leaf-like architecture with
419 high surface accessibility and an increased surface area. This structure facilitates effective contact
420 between the sorbent and the analytes, while the aromatic imidazole rings of ZIF-L can contribute
421 to π - π stacking interactions with the planar structures of aflatoxins. In addition, the nitrogen-
422 containing framework of ZIF-L may promote dipole-related interactions with the aflatoxin
423 molecules.

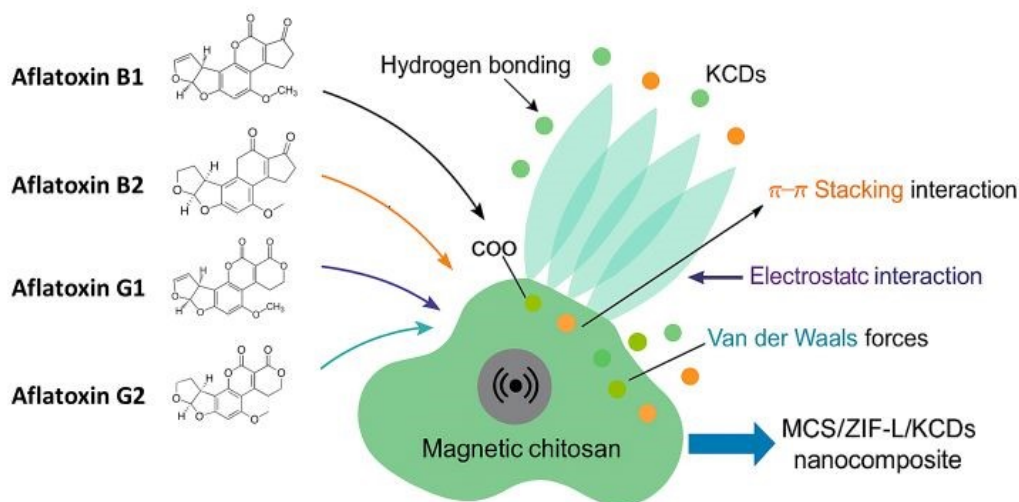
424 Furthermore, the incorporation of KCDs onto the MCS/ZIF-L composite surface provides
425 additional active sites enriched with oxygen-containing functional groups such as -OH, -COOH,
426 and C=O, as confirmed by FTIR and SEM-EDX analyses. These functional groups enhance the
427 interaction between the sorbent and aflatoxin molecules through hydrogen bonding, dipole-dipole
428 interactions, and van der Waals forces. The deposition of KCDs also increases the surface

1
2
3 429 roughness and heterogeneity of the composite, which can contribute to improved analyte
4
5 430 accessibility within the nanoscale structure.

6
7
8 431 The pH of the extraction medium plays an important role in the extraction efficiency. As
9
10 432 discussed in Section 3.2, the extraction recoveries increased from pH 3 to 7, remained nearly
11
12 433 constant between pH 7 and 8, and decreased at higher pH values. Therefore, PBS buffer solution
13
14 434 (pH = 7.4) was selected as the optimal extraction medium. This observation is consistent with the
15
16 435 experimentally determined pHPZC value of 7.3 for the MCS/ZIF-L/KCDs sorbent (Fig. S1),
17
18 436 indicating that the sorbent surface is close to electrically neutral under near-neutral conditions.
19
20 437 Such conditions favor effective interaction between the sorbent surface and aflatoxin molecules.

21
22 438 The rapid adsorption behavior observed during vortex-assisted extraction (optimal at 1.0 min)
23
24 439 suggests that the hierarchical structure of the composite provides readily accessible active sites
25
26 440 and facilitates fast mass transfer between the sorbent and analytes. After extraction, the magnetic
27
28 441 core enables rapid separation of the sorbent from the sample solution using an external magnet,
29
30 442 eliminating the need for filtration or centrifugation. The bound aflatoxins can then be efficiently
31
32 443 desorbed using methanol, whose polarity allows disruption of the sorbent–analyte interactions and
33
34 444 ensures effective recovery of the target compounds.

35
36
37 445 As a result, the multifunctional and hierarchical architecture of the MCS/ZIF-L/KCDs
38
39 446 nanocomposite provides multiple interaction pathways and a large accessible surface area,
40
41 447 resulting in efficient extraction and preconcentration of aflatoxins from complex food matrices.
42
43 448 The analytical merit of the proposed sorbent therefore arises from the synergistic integration of
44
45 449 magnetic chitosan, ZIF-L, and KCDs in a single composite structure, making it a robust and
46
47 450 versatile sorbent for the trace-level determination of aflatoxins in food samples (Scheme 1).
48
49
50
51
52
53
54
55
56
57
58
59
60



451

452 **Scheme 1** Schematic illustration of the proposed extraction mechanism of aflatoxins B1, B2, G1, and G2
 453 using the MCS/ZIF-L/KCDs nanocomposite.

454 3.8. Application of the Method

455 To consider the ability of the MCS/ZIF-L/KCDs-MD- μ SPE coupled with HPLC-FLD to be
 456 used in various matrices, for simultaneous preconcentration/separation and determination of
 457 aflatoxins B1, B2, G1, G2, was studied in ziziphus jujube, wheat, corn, white rice, pistachio, and
 458 walnut. To investigate the accuracy of the method, the concentrations of 50, 100, and 200 ng Kg⁻¹
 459 of aflatoxins B1, B2, G1, and G2 were spiked in Ziziphus jujube. The relative recoveries (%) of
 460 91.0-99.4 were obtained with RSDs (%) \leq 3.5 (n=3). The results are indicated in Table 2. The
 461 Ziziphus jujube HPLC chromatograms are revealed in Fig. 4.

462

463

464

Table 2 Application of MCS/ZIF-L/KCDs -D μ SPE for simultaneous separation and determination of aflatoxin B1, B2, G1, G2 in different real samples.

Sample	Spiked concentration (ng Kg ⁻¹)				Founded concentration (ng Kg ⁻¹)				Relative recoveries (%)			
	B1	B2	G1	G2	B1	B2	G1	G2	B1	B2	G1	G2
Ziziphus jujube ^a	-	-	-	-	N.D.	N.D.	N.D.	N.D.	-	-	-	-
	10	10	10	10	9.5 ^b ±3	9.8±0.5	9.3±0.6	9.4±0.4	95.0	98.0	93.0	94.0
	50	50	50	50	49.3±2.7	48.6±2.6	49.0±2.5	48.3±3.0	98.6	97.2	98.0	96.6
	100	100	100	100	97.5±3.1	95.3±3.2	98.7±2.9	96.5±2.9	97.5	95.3	98.7	96.5
Wheat	-	-	-	-	N.D.	N.D.	N.D.	N.D.	-	-	-	-
	10	10	10	10	9.4±0.	9.5±0.6	9.4±0.2	9.6±0.5	94.0	95.0	94.0	96.0
	50	50	50	50	48.2±2.4	49.6±3.2	47.5±3.5	48.8±2.3	96.4	99.2	95.0	97.6
	100	100	100	100	99.1±2.4	96.6±2.5	94.8±2.3	95.1±2.5	99.1±2.7	96.6	94.8	95.1
Corn	-	-	-	-	N.D.	N.D.	N.D.	N.D.	-	-	-	-
	10	10	10	10	9.60±0.5	9.90±0.5	9.20±0.4	9.70±0.6	96.0	99.0	92.0	97.0
	50	50	50	50	49.1±2.5	49.5±2.2	47.6±2.8	48.0±3.5	98.2	99.0	95.2	96.0
	100	100	100	100	96.2±2.8	98.9±2.6	97.2±3.3	98.5±3.2	96.2	98.9	97.2	98.5
White Rice	-	-	-	-	N.D.	N.D.	N.D.	N.D.	-	-	-	-
	10	10	10	10	9.10±0.5	9.50±0.4	9.30±0.6	9.20±0.5	91.0	95.0	93.0	92.0
	50	50	50	50	48.3±2.3	48.6±2.5	47.5±2.6	49.1±2.2	96.6	97.2	95.0	98.2
	100	100	100	100	98.6±2.4	97.2±3.2	97.8±2.6	99.4±2.1	98.6	97.2	97.8	99.4
Pistachio	-	-	-	-	N.D.	N.D.	N.D.	N.D.	-	-	-	-
	10	10	10	10	9.00±0.6	9.40±0.4	9.60±0.5	9.30±0.4	90.0	94.0	96.0	93.0
	50	50	50	50	47.6±2.3	48.2±2.0	46.5±2.9	46.9±2.5	95.2	96.4	93.0	93.8
	100	100	100	100	94.1±3.0	96.8±3.1	97.8±2.6	96.2±2.8	94.1	96.8	97.8	96.2
Walnut	-	-	-	-	N.D.	N.D.	N.D.	N.D.	-	-	-	-
	10	10	10	10	9.00±0.3	9.30±0.5	9.50±0.6	9.10±0.5	90.0	93.0	95.0	91.0
	50	50	50	50	48.3±2.5	49.1±2.1	48.5±2.5	47.7±2.2	96.6	98.2	97.0	95.4
	100	100	100	100	97.1±3.1	98.6±2.6	99.0±2.2	98.5±2.5	97.1	98.6	99.0	98.5

^a Ziziphus jujube, wheat, corn, white rice, pistachio, and walnut were all purchased from a local supermarket in Isfahan, Iran.

^b The obtained data are the mean of three replicates.



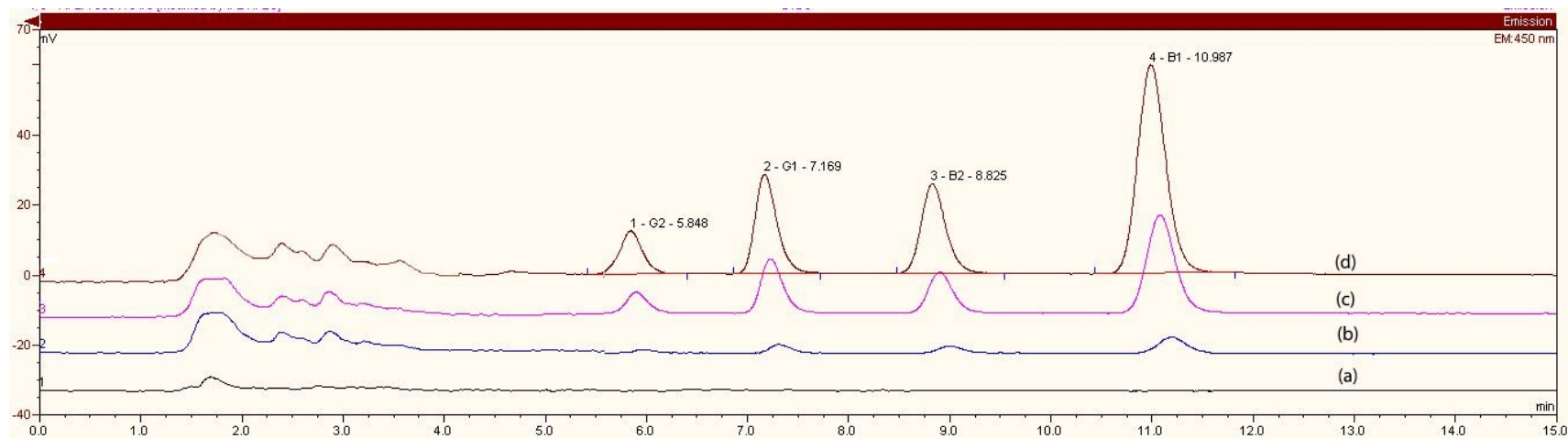


Fig. 4 HPLC-FLD chromatograms of aflatoxins B1, B2, G1, and G2 in *Ziziphus jujuba*; **a**) blank sample, and the spiked levels of **b**) 10, **c**) 50, and **d**) 100 (ng Kg⁻¹) after applying the method.

3.9. Comparison of the Proposed Method

To evaluate the analytical performance of the proposed MCS/ZIF-L/KCDs-MD- μ SPE method, its figures of merit were compared with representative previously reported methods, as summarized in Table 3. Since the published methods differ in sorbent composition, extraction format, sample matrix, and validation conditions, the comparison should be considered descriptive rather than statistically inferential. Nevertheless, the proposed method exhibited low detection limits (0.002–0.003 $\mu\text{g kg}^{-1}$), satisfactory recoveries, and good precision ($\text{RSD} \leq 3.0\%$), demonstrating that it is analytically competitive and well suited for the separation, preconcentration, and determination of aflatoxins in complex food matrices.

Table 3 Comparison of the proposed method with some recent studies for the simultaneous extraction and determination of aflatoxin B1, B2, G1, and G2 in foodstuffs.

Method	Adsorbent	Sorbent amount (mg)	Matrix complexity	Detection technique	LDR ($\mu\text{g Kg}^{-1}$)	LOD ($\mu\text{g Kg}^{-1}$)	RSD (%)	Extraction time (min)	Reusability	Ref.
MD- μ SPE	MCS/ZIF-L/KCDs nanocomposites	25.0	Ziziphus jujube, wheat, corn, white rice, pistachio, walnut	HPLC-FLD	0.01-1000	0.002,0.003	≤ 3.0	1.0	6.0	This study
MD- μ SPE	Sp-M-Dpi ^a	150	Pistachio	HPLC-FLD	2.0-10.0	0.02-0.07	< 5.4	1.0	-	37
MD- μ SPE	Dummy template MIP	55.0	Nuts, grains	HPLC-FLD	0.15-100	0.059–0.208	< 5.4	< 35	8.0	38
SPE	Activated carbon-boron	5.0	Pistachio, walnut, cashew, nut	HPLC-FLD	0.12-0.10	0.04-0.16	< 7.0	3.0	10.0	39
MSPE	Fe ₃ O ₄ @SiO ₂ @TiO ₂ APTMS-CPA	10.0	Hazelnut, peanut, almond	HPLC-FLD	0.09-12.0	0.05-0.13	< 7.1	4.0	8.0	40
SPE	skeleton of polystyrene–polyvinyl pyrrolidone nanofiber	20.0	plant- and animal-based food samples	HPLC-FLD	0.5-5.0	0.07–0.17	< 8.0	5.0	-	41

^aSp-M-Dp: polydopamine-coated magnetic spirulina nanocomposite

475

476

477

478

479 4. Conclusion

480 In this study, a novel MCS/ZIF-L/KCDs granular–leaf hybrid nanocomposite was successfully
481 synthesized and applied as an efficient sorbent for MD- μ SPE of aflatoxins B1, B2, G1, and G2
482 from ziziphus jujube, wheat, corn, white rice, pistachio, and walnut samples before HPLC-FLD
483 determination. The developed method exhibited several advantages, including low consumption
484 of organic solvents and sorbents, rapid extraction, and simple operation. Green analytical
485 chemistry evaluation using AGREE, AGREEprep, and BAGI confirmed the environmentally
486 friendly nature of the proposed procedure. Furthermore, the method demonstrated satisfactory
487 analytical performance, including wide linear ranges, acceptable precision, and low detection
488 limits. The obtained results indicate that the MCS/ZIF-L/KCDs-based MD- μ SPE coupled with
489 HPLC-FLD provides a reliable, sensitive, and environmentally friendly strategy for the separation,
490 preconcentration, and determination of aflatoxins in grain and nut samples. Therefore, the
491 developed method shows strong potential for application in routine food safety monitoring and
492 quality control of mycotoxin contamination.

493 Conflicts of interest

494 The authors declare no conflict of interest.

495 Acknowledgements

496 The authors gratefully appreciate the University of Jiroft and Erciyes University for their valuable
497 support of this research study.

498 References

- 1
2
3 499 1 F. Moghadasi, S. Roudbarmohammadi, S. Amanloo, F. Nikoomanesh and M. Roudbary,
4 *Mol. Biol. Rep.*, 2024, 51, 53.
5
6
7 501 2 B. Balan, A. S. Dhaulaniya, M. Kumar, M. Kumar and P. Kumar, *Food Saf Health*, 2024,
8 2, 39–71.
9
10 503 3 H. F. Hassan, K. Zgheib, C. F. Iskandar, A. Chalak, N. Alwan and M. G. Abiad, *Sci. Rep.*,
11 2024, 14, 25761.
12
13 505 4 A. Jallow, H. Xie, X. Tang, Z. Qi and P. Li, *Compr. Rev. Food Sci. Food Saf.*, 2021, 20,
14 2332–2381.
15
16 507 5 A. Kumar, H. Pathak, S. Bhadauria and J. Sudan, *Food Prod Process Nutr*, 2021, 3, 17.
17
18 508 6 V. Navale, K. R. Vamkudoth, S. Ajmera and V. Dhuri, *Toxicol. Rep.*, 2021, 8, 1008–1030.
19
20 509 7 K. Mukhtar, B. G. Nabi, S. Ansar, Z. F. Bhat, R. M. Aadil and A. Mousavi Khaneghah,
21 *Toxicon*, 2023, 232, 107227.
22
23 511 8 K. Zhang, B. Flannery and L. Zhang, *J. Agric. Food Chem.*, 2024, 72, 8380–8388.
24
25 512 9 M. Carvajal-Moreno, *J. Cereal Sci.*, 2022, 103, 103293.
26
27 513 10 L. Shi, A. Li, Y. Xu, H. Yang and G. Yang, *Microchim Acta*, 2025, 192, 307.
28
29 514 11 A. Castell, N. Arroyo-Manzanares, P. Viñas, I. López-García and N. Campillo, *TrAC*
30 *Trends Anal Chem*, 2024, 178, 117826.
31
32 516 12 M. Shirani, S. Sepahi, O. Ozalp and M. Soylak, *Int. Dairy J.*, 2025, 165, 106210.
33
34 517 13 M. Shirani, F. Ansari, M. Shabaniyan, U. Wagenknecht, Q. Salamat, M. Faraji, M. Basij and
35 M. Adeli, *Microchem Journal*, 2024, 205, 111254.
36
37 519 14 J. Wei, P. Fan, Y. Huang, H. Zeng, R. Jiang, Z. Wu, Y. Zhang and Z. Hu, *Org Chem*
38 *Frontiers*, 2024, 11, 3459–3464.
39
40 521 15 M. Soylak, S. Sajjad, Q. Salamat and H. E. H. Ahmed, *Food Chem.*, 2025, 490, 145101.
41
42 522 16 S. Lu, Y.-J. Zhang, Y.-J. Cheng, Z.-H. Qin, G.-D. Wang, Y. Bai, Y. Lin, H. Wang, Y. Sui,
43 L. Hou and Y.-Z. Li, *J. Mater. Chem. A Mater.*, 2025, 13, 10581–10589.
44
45
46
47
48
49
50
51
52
53
54
55
56
57
58
59
60

- 1
2
3 524 17 S. N. Pandey, M. Afzal, A. Goyal, G. Padma Priya, B. Mohanty, K. Goyal, M. Rana and M.
4 Imran, *Inorg. Chem. Commun.*, 2025, 179, 114671.
5
6
7 526 18 S. Wang, L. Luo, A. Wu, D. Wang, L. Wang, Y. Jiao and C. Tian, *Coord. Chem. Rev.*, 2024,
8 498, 215464.
9
10
11 528 19 M. Maneesha, P. C. Preethi, A. Harisankar, T. G. Sreeja, V. K. Ratheesh Kumar, S. T. Veedu
12 and R. Raghunandan, *Microchem J*, 2025, 210, 113046.
13
14
15 530 20 L. Gao, H. Yang, Y. Lu, S. Chen, L. He and J. Liu, *Food Chem.*, 2024, 458, 140215.
16
17
18 531 21 L. Gao, Y. Lu, H. Yang, L. Guo, S. Chen and J. Liu, *Microchem J*, 2025, 210, 112961.
19
20
21 532 22 M. Ghorbani, M. Keshavarzi, M. Pakseresht, P. Mohammadi, A. Shams, A. Mehraban and
22 A. Ismailzadeh, *Anal. Bioanal. Chem.*, 2023, 415, 5681–5694.
23
24
25 534 23 G. Khalilipour, A. R. Karamibonari, M. Movassaghghazani, J. Shayegh and M. R. Afshar
26 Mogaddam, *Microchem J*, 2024, 202, 110806.
27
28
29 536 24 R. Atchudan, T. N. J. I. Edison, S. Perumal, R. Vinodh, A. K. Sundramoorthy, R. S. Babu
30 and Y. R. Lee, *Chemosensors*, 2021, 9, 166.
31
32
33 538 25 M. Shirani, A. Aslani, F. Ansari, E. Parandi, H. R. Nodeh and E. Jahanmard, *Microchem J*,
34 2023, 189, 108507.
35
36
37 540 26 R. Moradi, M. Seraji, N. P. Khalili, Q. Salamat and M. Soyak, in *Fundamentals and*
38 *Biomedical Applications of Chitosan Nanoparticles*, Elsevier, 2025, pp. 447–496.
39
40
41 542 27 C. J. Wijaya, S. Ismadji, H. W. Aparamarta and S. Gunawan, *Molecules*, 2021, 26, 4416.
42
43
44 543 28 J. He, Y. Xiong, H. Mu, P. Li, Y. Deng, W. Zou and Q. Zhao, *Crystals (Basel)*, 2023, 13,
45 544 564.
46
47
48 545 29 H. Li, Y. Cheng, J. Li, T. Li, J. Zhu, W. Deng, J. Zhu and D. He, *Nanomaterials*, 2022, 12,
49 546 4008.
50
51
52 547 30 X. Li, D. Zeng, Z. He, P. Ke, Y. Tian and G. Wang, *Carbohydr. Polym.*, 2022, 276, 118729.
53
54
55 548 31 M. Aslan and H. Eskalen, *Fuller Nanotub Car N*, 2021, 29, 1026–1033.
56
57
58
59
60

- 1
2
3 549 32 M. Xie, L. Zeng, Q. Zhang, Y. Kang, H. Xiao, Y. Peng, X. Chen and J. Luo, *J. Alloys*
4 550 *Compd.*, 2015, 647, 892–905.
- 551 33 K. S. Park, Z. Ni, A. P. Côté, J. Y. Choi, R. Huang, F. J. Uribe-Romo, H. K. Chae, M.
552 O’Keeffe and O. M. Yaghi, *Proc Natl Acad Sci*, 2006, 103, 10186–10191.
- 553 34 H. Li, Y. Zhang, S. Li, J. Shi, H. Wu, A. Jabbarzadeh, J. Liu, T. Cao, X. Fan and F. Zhou,
554 *Carbon N. Y.*, 2026, 246, 120869.
- 555 35 M. Shirani, Q. Salamat, M. Amirani Poor, H. M. Nejad and M. Soylak, *J Food Compos*
556 *Anal*, 2025, 142, 107388.
- 557 36 Q. Long, H. Zhao, T. Qiu, H. Wu, H. Yan and S. Qiu, *Colloids Surf. A Physicochem. Eng.*
558 *Asp.*, 2025, 727, 138247.
- 559 37 R. Karami-Osboo, F. Ahmadpoor, M. Nasrollahzadeh and M. Maham, *Food Chem.*, 2022,
560 377, 131967.
- 561 38 R. Thati, B. S. Seetha, P. Alegete and M. K. R. Mudiam, *Food Chem.*, 2024, 433, 137342.
- 562 39 H. S. Karapınar and A. Balıkçioğlu, *J Food Compos Anal*, 2022, 112, 104680.
- 563 40 H. S. Karapınar and A. Bilgiç, *J Food Compos Anal*, 2022, 105, 104261.
- 564 41 Y. Wang, L. Chu, J. Qu, B. Ding and X. Kang, *Food Chem.*, 2024, 436, 137699.
- 565

Open Access Article. Published on 16 May 2026. Downloaded on 4/6/2026 10:14:02 PM.
This article is licensed under a Creative Commons Attribution-NonCommercial 3.0 Unported Licence.



Data Availability Statement:

[View Article Online](#)
DOI: 10.1039/D6AY00202A

Due to the large volume of data generated from the calculations in this study and institutional restrictions on data sharing, the complete datasets cannot be made publicly available. However, the calculation scripts used in the research are available from the authors upon reasonable request.

1
2
3
4
5
6
7
8
9
10
11
12
13
14
15
16
17
18
19
20
21
22
23
24
25
26
27
28
29
30
31
32
33
34
35
36
37
38
39
40
41
42
43
44
45
46
47
48
49
50
51
52
53
54
55
56
57
58
59
60

Open Access Article. Published on 16 March 2026. Downloaded on 4/6/2026 12:44:02 PM.
This article is licensed under a Creative Commons Attribution-NonCommercial 3.0 Unported Licence.

